Tool axis adjustment for 5-axis roughing operations

Baptiste Jousselin, Yann Quinsat, Christophe Tournier

Tool axis adjustment for 5-axis roughing operations

B. Jousselin[a,b], Y. Quinsat[b], C.Tournier[a]

[a] *TOPSOLID, 7 rue du Bois Sauvage, 91055 Evry, France*
[b] *Université Paris-Saclay, ENS Paris-Saclay, LURPA, 91190 Gif-sur-Yvette, France*

Abstract

The increased accessibility of the tool achieved by using 5-axis roughing reduces the overall machining time of complex parts by reducing or eliminating the re-roughing and semi-finishing operations thereby decreasing the volume of remaining material before finishing operations. However, 5-axis milling generates significant variations in tool orientation which, combined with the high tool engagement in the material required by the roughing conditions, can be penalizing. Controlling these variations is therefore mandatory to guarantee the tool life, the productivity and the quality of the roughing operation. Thus, a multi-objective optimization is proposed to define the successive orientations of the tool axis along the path that minimize the feedrate slowdowns and thus the machining time, balance the pushing or pulling machining configurations and respect the programmed scallops heights of the machined surface. In this work, the tool path is defined by two curves, one constraining the position of the tool and the other its orientation allowing for a parametric synchronization to conduct the optimization. From the definition of the weights of each of the minimization objective functions, it is possible to find a tool axis orientation solution that satisfies the given constraints all along the path. The application on a test part by simulation and machining highlights the effectiveness of the proposed approach and the advantages of controlling the evolution of the tool axis orientation in 5-axis roughing.

Keywords: 5-axis machining, Roughing, Optimization, Tool axis orientation

1. Introduction

5-axis milling operations offer many advantages when machining complex cavities, including improved productivity due to increased tool accessibility compared to 3-axis operations. This makes it possible to reduce the path lengths and required tool lengths [1]. Mainly used for finishing operations, 5-axis milling can also prove beneficial in roughing by reducing the overall machining time and minimizing the volume of material remaining at the end of roughing [2].

Most of the strategies offered for 5-axis roughing use 5-axis simultaneous milling only in areas that cannot be machined in 3-axis milling. The local addition of 5-axis rework paths can, however, lead to abrupt changes in the radial engagement of the tool in the material: one part of the tool may be moving into an area where the material has already been removed while another is under high local load due to heavy engagement (*Figure 1*a).

Anticipating the tool orientation required during the last path on the flank helps to smooth out these engagement variations between successive radial paths and thus distribute the load applied to the tool more evenly along the cutting edge (*Figure 1*b). It is then necessary to generate a continuous 5-axis trajectory for the entire roughing operation.

In contrast to the finishing operation, which concentrates on the sweeping of surfaces, roughing is applied to the removal of volumes. The engagement values of the tool with the workpiece are then much greater and might present risks for the part and the tool if they are not controlled [3]. This control is all the more crucial during multiaxial roughing, during which tool orientation variations can be significant.

These variations in the orientation of the tool axis affect the machining process in several ways. The first one concerns the smoothness of the tool path and its consequences on the manufacturing time and the kinematic behavior of the machine tool. The major works on this subject deal with the smoothing of tool paths in a context of finishing. Several techniques for global smoothing of the successive orientations of the tool axis have been proposed in order to improve the kinematic performances of the machine-tool axes and especially rotary axes. In the part space by including kinematic constraints of the machine tool such as axes jerk or tangential jerk in [4, 5], by minimizing the shortest path between angular configurations [6, 7], or by minimizing the variations in the acceleration of the machine's rotary axes [8, 9]. However, the smoothing of the trajectory in the joint space makes it difficult to control the orientation and positioning of the tool with respect to the workpiece. The deviations of the path must be controlled, especially in the case of flank milling, to minimize geometrical deviation of the machined surface as proposed in [10] for global smoothing and in [11] for corner smoothing. However, the dependency of these methods on the kinematic configuration of the machine tool is a disadvantage for the development of a CAM solution that is sufficiently cross-functional and independent of the machine tool and CNC control used. The optimization of the orientation of the tool axis in the coordinate system associated to the part is therefore preferable from this point of view [12, 13].

Email address: christophe.tournier@ens-paris-saclay.fr (C.Tournier)

Global smoothing strategies in the part space have been developed to limit abrupt changes in the orientation of the tool axis along a path [14]. These methods improve the kinematic performance of the machine axes, but do not optimize the orientation of the tool axis with respect to the workpiece. When roughing a cavity, tilt optimization must be conducted by considering both the orientation of the tool with respect to the flank and bottom surfaces to ensure that the part geometry is respected.

Variations in the orientation of the tool axis also have a direct effect on the quality of the bottom surface and the volume of material remaining [15]. Indeed, combined with the geometries of the cylindrical or toric tools commonly used in roughing, these variations will generate scallops of varying heights on the bottom surfaces during roughing. It is therefore necessary to control these variations in order to guarantee the most regular excess thickness possible to avoid or minimize the semi-finishing operations. In the same way, controlling the orientation of the tool axis in relation to the part allows the management of local and global collisions [16].

Finally, the orientation of the tool axis also has a direct influence on the cutting forces experienced by the tool [17] which are strongly linked to the cutter workpiece engagement. However, determining the continuously changing cutter workpiece engagement remains a challenge, especially for toroidal and flat-end cutters during 5-axis roughing and semi-finish milling of sculptured parts [18], and is out of the scope of this paper. Thus, depending on whether the tool is working with a positive (pulling) or negative (pushing) tilt angle, the distribution of forces on the tool will be different, as will its dynamic behavior in terms of the generation of vibrations. The tool life, especially in hard materials, is closely related to these cutting conditions.

The strategy developed in this article therefore aims at controlling the tool posture with respect to the part during a 5-axis roughing operation in order to ensure productivity, surface quality and operating conditions the tool. The evolution of the tool axis orientations during a pocket roughing operation on a 5-axis machining center is optimized in order to respect these criteria through a compromise between the smoothness of the tool path axis behavior along the tool path and the programmed tilt angle between the tool axis and the surface being machined. Lastly, the kinematic characteristics of the CNC machine such as max. velocity, max. acceleration and max. jerk of the axes are not directly taken into account in order to remain independent from the machine used.

The rest of the paper is organized as follows: the calculation of the guide curves used for the minimization of the objective function and the determination of the adjusted tool orientations is explained in section 2. The determination of tool axis orientations is presented in section 3, then the minimization of the objective function is described in section 4. The application of the proposed method to the roughing of a pocket is presented in part 5 before concluding remarks on the benefits of this method in the last section.

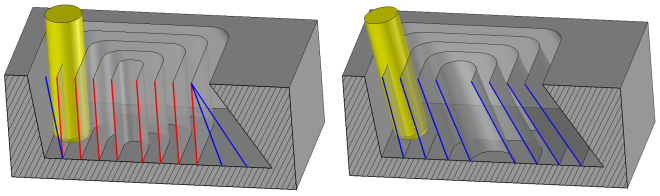

a) 3-axis with 5-axis re-roughing b) 5-axis smooth tilting

Figure 1: Evolution of the radial engagement of the tool between successive tool paths

2. Orientation of the tool axis by synchronization of the guide curves

In order to control the orientation of the tool axis and to ensure that it evolves continuously (*Figure 1*b), the tool is considered to be guided by 2 curves (*Figure 2* a): the path curve $C_P(s_P)$ with $s_P \in [0,1]$, is the intersection of the tool axis with the end machined surface, and the tilting curve $C_T(s_T)$ with $s_T \in [0,1]$, is the location of another point belonging to the tool axis to orient it. These two curves are constructed from the geometry of the pocket (bottom and flanks) so as to follow as closely as possible the geometry of the flank surfaces during the last radial pass, and thus remove as much material as possible during the roughing phase with a continuous evolution of the radial engagement of the tool [19].

The guide curves defined in this way allow the orientation of the tool axis to be constrained in the plane orthogonal to the feed direction (*Figure 2*b). However, a degree of freedom still has to be defined in the feed plane to fully constrain the tool orientation. The tool is then moved along the resulting axis until it contacts the end-machined surface to determine the position of the tool center (*Figure 2*c). The whole part of the calculation of the tool axis orientation is therefore performed without the exact knowledge of the position of the contact point of the tool with the end machined surface. Both the path and the tilt curves are oriented with a starting point set to s_{P0} and s_{T0} (*Figure 3*).

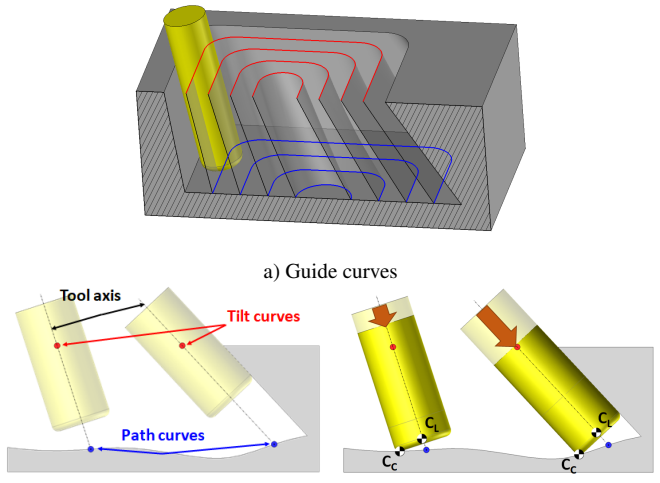

a) Guide curves

b) Tool axis orientation computation c) Cutter location point computation

Figure 2: Tool axis guiding along 2 curves

The orientation of the tool axis u with respect to the end-machined surface is set by the yaw (θ_n), roll (θ_f), and tilt θ_t) angles, defined in the (C_C, $\mathbf{f}$, $\mathbf{n}$, $\mathbf{t}$) frame. C_C is the contact point between the tool and the end-machined surface, $\mathbf{f}$ is the feed direction of the tool with respect to the surface, $\mathbf{n}$ is the surface normal to the point C_C, and $\mathbf{t}$ is the vector product between $\mathbf{f}$ and $\mathbf{n}$. An approximation on the evaluation of the contact normal is then performed in order to simplify the calculations. As shown in *Figure 3*, the ($\mathbf{f}$, $\mathbf{n}$, $\mathbf{t}$) basis is computed at the $P_{P(s_P)}$ point of the path curve and not at the real contact point C_C, whose position is still unknown. This approximation is equivalent to considering that the orientation of the surface normal varies little in a defined area to within one tool radius.

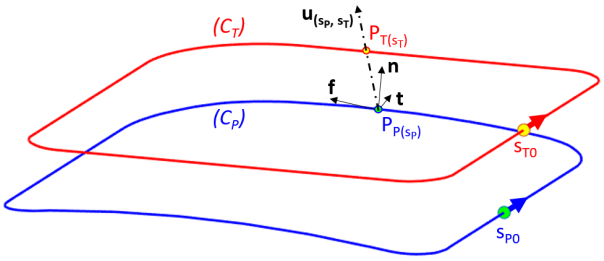

Figure 3: Tool axis orientation setting

Since θ_f is already constrained by the fact that the tool axis has a point on C_P and a point on C_T, simply setting θ_t will constrain the tool orientation. The problem is therefore to find the values of curvilinear abscissa s_P and s_T to obtain the desired orientation (*Equation 1*).

$$\theta_t = \frac{\mathbf{u}_{(\mathbf{s_P},\mathbf{s_T})} \cdot \mathbf{f}}{|\mathbf{u}_{(\mathbf{s_P},\mathbf{s_T})} \cdot \mathbf{f}|} \arccos\left(\frac{(\mathbf{u}_{(\mathbf{s_P},\mathbf{s_T})} - (\mathbf{u}_{(\mathbf{s_P},\mathbf{s_T})} \cdot \mathbf{t}) \cdot \mathbf{t}) \cdot \mathbf{n}}{\left\| \mathbf{u}_{(\mathbf{s_P},\mathbf{s_T})} - (\mathbf{u}_{(\mathbf{s_P},\mathbf{s_T})} \cdot \mathbf{t}) \cdot \mathbf{t} \right\|} \right) \quad (1)$$

This is achieved by synchronizing the curves, *i.e.* correlating the curvilinear abscissa values of C_P and C_T to generate the successive tool axes over the entire trajectory. The uniform parametric synchronization consists in making s_P and s_T evolve according to the same and unique parameter $s \in [0, 1]$.

3. Optimization of the guide curves synchronization

3.1. Definition of the objective function

The linear evolution of the curvilinear abscissa provided by the uniform parametric synchronization is not efficient enough to control the evolution of the tool orientation. A finer model must therefore be used to control more precisely the evolution of the curvilinear parameters s_P and s_T which are characterized by the distribution functions g_P and g_T (*Equation 2*).

$$\forall s \in [0,1], \begin{cases} s_P = g_P(s) = \sum_{i=0}^{n_T=3} c_{(P,i)} \cdot s^i \\ s_T = g_T(s) = \sum_{i=0}^{n_D=3} c_{(T,i)} \cdot s^i \end{cases} \quad (2)$$

Cubic functions were chosen in order to provide an inflection point which allows limiting the evolution of the parameter on one curve compared to the other and thus to adjust the orientation of the tool. Also, all the values (s_P, s_T) which define the orientation of the tool can be obtained by the sole determination of 8 parameters: 4 coefficients $c_{(P,i)}$ and 4 coefficients $c_{(T,i)}$ ($i \in [0, 3]$).

The first considered objective in the search for these 8 coefficients is to maintain the orientation of the tool within an angular range $[\theta_{tmin}, \theta_{tmax}]$ defined according to the desired machining conditions (*Figure 4*a) and so that there are no collisions between the tool and the workpiece. For example, machining at θ_t strictly negative or strictly positive avoids transitions between machining by pushing and pulling along the tool path, which allows a better control of the dynamic behavior of the tool and ensures its lifetime. Thus, the length L_{HL} traveled by the tool outside the angular range has to be minimized and is expressed as (*Equation 3*):

$$L_{HL} = \int_s |\theta_t(s) - \frac{\theta_{tmax} + \theta_{tmin}}{2}| \cdot H(s) \cdot ds \quad (3)$$

Where H takes the value 1 when the orientation of the tool is outside the limits, or 0 otherwise (*Equation 4*).

$$H(s) = \begin{cases} 1 \; if \; |\theta_t(s) - \frac{\theta_{tmax}+\theta_{tmin}}{2}| \geq \frac{\theta_{tmax}-\theta_{tmin}}{2} \\ 0 \; otherwise \end{cases} \quad (4)$$

Compared to a strict constraint of working within the angular range, the use of this function allows keeping solutions that may locally exceed the limits but offer degrees of freedom to the other objectives presented below.

The observance of an operating angular range can also lead to abrupt angular variations that can affect the kinematic performance of the machine axes during path traversal. Indeed, significant variations in the orientation of the tool axis induce large amplitude movements of the machine tool's rotary axes that may affect the actual feedrate. Thus, the quadratic sum of the angular variations along the curvilinear abscissa (*Figure 4*b) is used to quantify the smoothness criterion E_s (*Equation 5*).

$$E_s = \int_s \left| \frac{\partial \theta_t}{\partial s}(s) \right|^2 \cdot ds \quad (5)$$

Although an angular range is specified, more precise control of the tilt angle along the trajectory may be desired (*Figure 4*c), in particular to control the variations of scallop height on the last axial level which realize the bottom surface. The quadratic sum of the deviations to an objective angle θ_{tobj} is defined as the tilting criterion E_t (*Equation 6*).

$$E_t = \int_s \left| \theta_{tobj} - \theta_t(s) \right|^2 \cdot ds \quad (6)$$

Finally, the global objective function F_{obj} of the optimization problem is the sum of the introduced targets, balanced with the weight β of the limits criterion, the weight φ of the smoothness criterion, that could be adapted to the kinematic performance of a given machine, and the weight τ of the tilting cri-

terion. The setting of these weights allows balancing the importance to give to each criterion in function of the case to face (*Equation 7*).

$$F_{obj} = \beta \cdot L_{HL} + \varphi \cdot E_s + \tau \cdot E_t \tag{7}$$

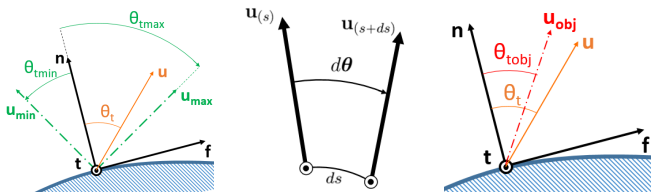

a) Bounds β b) Smoothness φ c) Tilting τ

Figure 4: Optimisation targets

As each tool path can be different, it is difficult to propose a standardization of the three weights given that the orders of magnitude of the objective functions can be very different. The choice of weights must be made by the operator in order to define the particular setting that is appropriate for his application.

The synchronization is thus defined by the 8 coefficients $c_{P,i}$ and $c_{T,i}$ ($i \in [0,3]$) which minimize the objective function under technological constraints which ensure the travel of the total trajectory. Indeed the evolution of the curvilinear abscissa on each curve must be increasing, and never be constant simultaneously on both curves, to ensure that the tool always progresses on the path (*Equation 8*). It is also important that the range of computed abscissa values allows at least the totality of the guide curves to be covered from the starting point set by the user (*Equation 9*).

$$\forall s \in [0,1], \begin{cases} \dot{g}_P(s) \geq 0 \\ \dot{g}_T(s) \geq 0 \\ \dot{g}_P(s) + \dot{g}_T(s) > 0 \end{cases} \tag{8}$$

$$\begin{cases} g_P(1) - g_P(0) \geq 1 \\ g_T(1) - g_T(0) \geq 1 \\ g_P(0) = 0 \end{cases} \tag{9}$$

All the objective functions are defined from the positioning of the tool in the part coordinate system in order to be independent of the machine tool used. However, this means that the kinematic modeling of the machine is not taken into account and that effects linked to singular positions may occur and must be verified a posteriori.

3.2. Optimization method

The optimization problem tackled previously reveals solving difficulties due to its definition as a multi objective, non linear, and with non linear constraints problem. The Sequential Quadratic Programming (SQP) algorithm is able to solve this kind of problem. This algorithm is applied to solve the optimization issue defined in *Equation 10*, which aims to minimize a non linear differentiable function f under constraints represented by the g function.

$$\begin{cases} minf(x), & f : \begin{pmatrix} \mathbb{R}^8 & \longrightarrow \mathbb{R} \\ c_{[P,T],[1,4]} & \longrightarrow F_{obj} \end{pmatrix} \\ g(x) \leq 0, & g : \begin{pmatrix} \mathbb{R}^8 & \longrightarrow \mathbb{R}^6 \\ c_{[P,T],[1,4]} & \longrightarrow g(x) \end{pmatrix} \end{cases} \tag{10}$$

with $g(x)$ defined from *Equation 8* and *Equation 9*.

This algorithm allows solving non-linear constrained optimizations and is particularly efficient in trajectory optimization calculations [20]. Iterating by local descent, the result however shows a strong dependence on the choice of the initial guess. Consequently, the initial guess should give acceptable tool axis orientation results. It is then chosen as the non-optimized path, namely the uniform parametric synchronization. In this initial configuration, all the reparameterization polynom coefficients are set to 0, excepted the first order ones which are equal to 1, which means that $g_P(s) = g_T(s) = s$.

3.3. Trajectory computation

The inputs required to compute the entire optimized trajectory are the optimization weights (β, φ, τ) to define the machining case, the guide curves C_P and C_T, the machining tolerance to fix the maximum distance between two successive C_L points, the target tilt angle and associated boundaries. The coordinates of the entrance point may be declared but remain optional since the latter point is automatically chosen in the most accessible area.

The SQP optimization gives the optimized reparameterization polynomials of the guide curves considering the weighting strategy. These polynomials are then used to compute the adjusted curvilinear abscissas for each guide curve, s_P and s_T (*Equation 2*).

Tool axis orientation is evaluated for each couple of points $(P_{P(s_P)}, P_{T(s_T)})$ and interpolated along the guide curves in order to respect the machining tolerance required. As there could be an interference between the tool and the bottom surface when changing the orientation of the tool, the positioning of the tool is recalculated after the parameterization of the curves, similar to the one described in figure *Figure 2*c. The C_C points are then evaluated to compute the final list of C_L points which, associated with the tool axis orientations at each point, define the complete trajectory (*Figure 5*).

Due to the SQP solving, the results are particularly dependent on the initial guess fixed for the optimization. If the entrance point is chosen in an area which is too hardly accessible by the tool, the optimization will converge but might result in tool axis orientations that are senseless considering a physical tool with a finite cutting length, or regarding the evolution of the tool engagement.

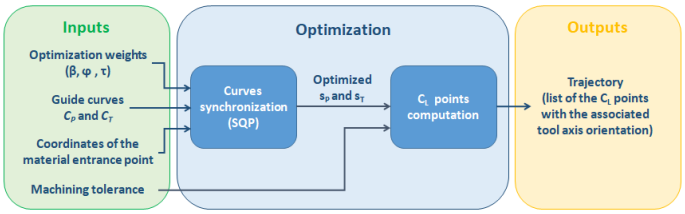

Figure 5: Optimized trajectory computation steps

3.4. Optimization example

The optimization example presented in *Figure 6* illustrates an optimization on 3 objectives ($\beta = 15, \varphi = 1.2, \tau = 1$) with predominantly respect of the operating range $[0°, 3°]$. The found coefficients give a new distribution of the curvilinear abscissa s_P and s_T (*Figure 6*b) which allows to remain within the chosen angular range (*Figure 6*a).

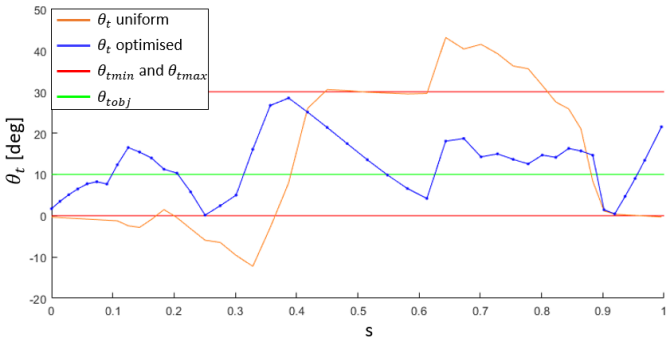

a) Constraints evolution

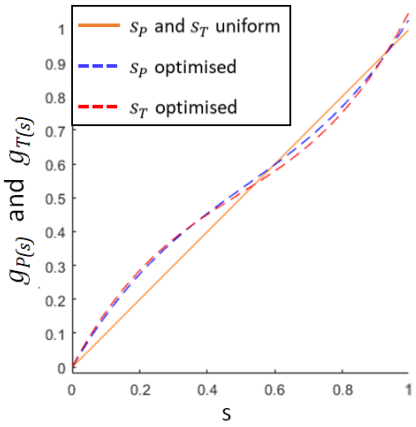

b) Distribution of curvilinear abscissa

Figure 6: Example of a multi-objective optimization

4. Experimental investigations

The proposed tool axis orientations adjustment approach has been applied to the trajectories of a complete axial roughing level of a closed pocket with large undercut areas (*Figure 7*) considering several weighting scenarios in the optimization problem:

- case 1: uniform parametric synchronization ($\beta = 0, \varphi = 0, \tau = 0$),
- case 2: machine axes smoothness optimization ($\beta = 0, \varphi = 1, \tau = 0$),
- case 3: limits optimization in $[-30°, 0°]$ ($\beta = 1, \varphi = 0, \tau = 0$),
- case 4: smoothness optimization in $[-45°, 0°]$ ($\beta = 5, \varphi = 10, \tau = 0$).

The angular ranges of the two latest optimization tests ensure negative values for the tilt angle of the tool in order to reduce the bending stresses on the tool [17], and then the vibrations of the subsystem composed of the tool, the tool-holder, and the spindle. It can be noted that the tool length is quite long ($L_c = 41\ mm$) to guarantee the roughing of the whole cavity. Combined with the high ratio between the tool-holder's length and its diameter required to increase accessibility ($L = 192\ mm$, $D = 27\ mm$), this does not favor the subsystem stiffness. The tilt angle optimization is not introduced yet because the optimal tilt angle is unknown for the tool and the material used. Therefore the tilt angle at the entrance point is set to 0.

Based on the orientations obtained for each different values of β, φ and τ, the paths have been simulated with the CAD/CAM software TopSolid'Cam, then tested in real machining conditions on a 5-axis machine tool Mikron UCP 710 whose structure according to the ISO10791 standard is:

$$V[w\ C'\ A'\ b\ X_m\ Y_m\ Z_m\ (C1)\ t]$$

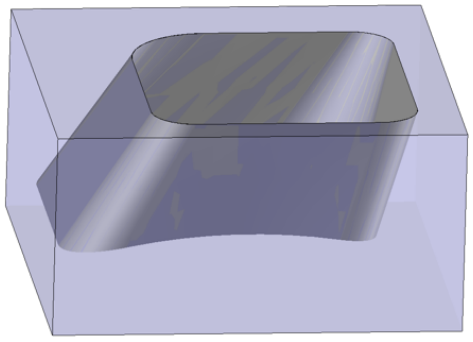

a) Representation of the test pocket

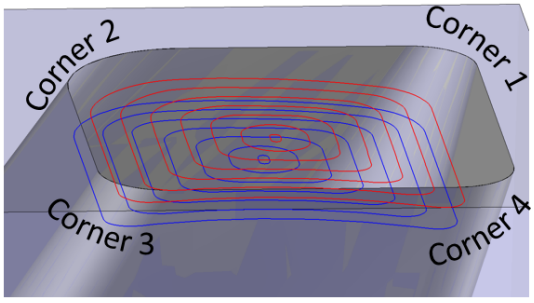

b) Computed guide curves

Figure 7: Test pocket and guide curves along one axial level of roughing

The G-Codes are spawned thanks to a post-processor developed by TopSolid and result in about 1800 to 3400 lines (tool location point) for an entire axial level, depending on the weighting strategy selected for the optimization. Given a computation time of approximately $10ms$ per tool location point on the tool path, the total computation time varies between 20s and 30s on a laptop computer.

The closed pocket is machined in a 2017A aluminium alloy stock with a FRAISA AluSpeed C5275.450 toroidal tool (diameter $D = 10\ mm$, corner radius $r_c = 1.5\ mm$, cutting length $L_c = 11\ mm$, number of teeth $Z = 2$) with the cutting conditions recommended by FRAISA for grooving. The maximum axial and radial engagements have been set to 4 mm and 4.5 mm respectively. The feed per tooth is set to $f_z = 0.08\ mm$, the spindle speed to $N = 15000\ rpm$ and the feedrate to $F = 2400\ mm/min$.

The spindle is instrumented with two Bruël & Kjær accelerometers (sensibility of 10.1 mV/g), positioned respectively along the **X** and **Y** directions (*Figure 8*a), in order to observe the evolution of the vibratory phenomena (*Figure 8*b). The acquired data are treated with the National Instruments system NI 9233.

They are supplemented with the servo traces analysis of the Siemens 840D controller, which gives access to articular positions and speeds of the machine axes during the machining experimentation. The velocities of the 5 axes (X,Y,Z,A,C) of the machine-tool during the machining experimentation have been recorded and the effective tangential velocity of the tool with respect to the workpiece F (feedrate) has been computed by using the forward kinematics. Since the maximal acquisition time of the CNC is about 20 s, the measurement of machining times and vibrations is only performed during the most constraining path, *i.e.* all along the last path on the pocket flank. The results are listed in *Table 1*. Figures 9 to 12 show the evolution of θ_t, effective feedrate F, and amplitude of the spindle vibrations on X and Y as a function of time.

The synchronization of the different data is done by identifying the first point of entry in the material of the trajectory on each recording and by correlating all the results of this identification. For the vibration analysis, a vibration peak is noted when the tool enters the material and allows to locate the entry point in the material.

In order to locate the measured phenomena on the CAD part, the four corners of the cavity are numbered in the order of tool traveling (*Figure 7*) and identified on the results graphs (Figures 9 to 12).

Numerous vibratory areas can be noted on the results of the uniform parametric synchronization strategy (case 1), especially in the corners where the fluctuations of θ_t are significant (*Figure 9*) and where the immersion of the tool increases and causes chatter. While no issue was encountered during the machining of the aluminium alloy stock, it could be risky for the tool to apply such a strategy in harder material like in titanium or nickel alloys. Indeed, the multiple inversions in the sign of θ_t would generate a rear gouging of the tool.

The smoothness optimization (case 2) provides a decrease in the machining time of more than 20 % compared to the non optimized strategy, despite having the same path length which is in line with what one would expect. Improved smoothness of the motion also reduces the excitation of machine modes hence reduces the inertial vibrations at tool path locations where the drives have sharp motion changes. Thus, even if the maximum amplitude of the vibrations is greater, the portions of the trajectories subjected to these vibrations are much less numerous. At last the results for this strategy highlight that vibratory phenomena does not occur systematically in the corners but also along the side of the pocket.

The limits optimization (case 3), aiming to keep the values of the tool axis orientation in a preferred range chosen here among negative values, results in a mitigation of the vibration waves all along the path (*Figure 11*) compared to the uniform parametric synchronization strategy (*Figure 9*). The explanation and the modeling of this observed dynamic behavior are part of the perspectives. Though, this strategy increases the machining time by more than 20 % compared to the uniform parametric synchronization. Its effects are then literally opposed to the smoothness optimization, especially in corner 3 where the machining time is almost three times longer.

The balance found with the combined optimization (case 4) induces a loss of productivity of 11 % compared to the uniform parametric synchronization strategy. However, this strategy remains more efficient than the limits optimization (case 3), whose the speed up percentage is more than twice as low. Moreover, the vibratory phenomena are removed all along the path, excepted around the corner 2 where the maximal amplitude of vibrations is still much lower than that of the smoothness opti-

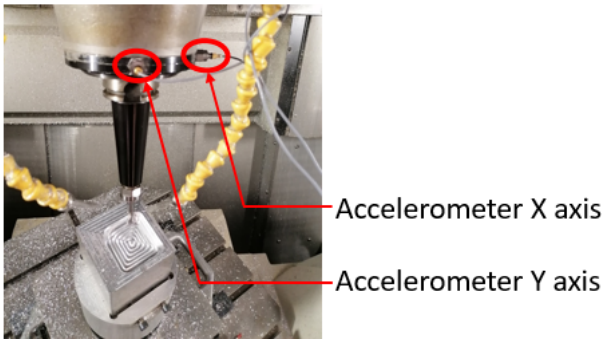

a) Accelerometer positioning

b) Machined surfaces

Figure 8: Spindle instrumentation and consequences of vibrations in corners

Objective	Weighting			Amplitude	Time	SpeedUp	Max. scallop	Remaining mat.
	β	φ	τ	$[m.s^{-2}]$	$[s]$	$[\%]$	$[mm]$	$[\%]$
case 1: Uniform	0	0	0	1426	14.5	0	1.95	1.42
case 2: Smoothness	0	1	0	1672	11.4	21.4	2.39	1.20
case 3: Limits	1	0	0	569	17.9	-23.4	1.81	1.15
case 4: Combined	5	10	0	1181	16.1	-11	2.2	0.6

Table 1: Evolution of the criteria according to the optimization parameters

mization. A combination between the weights β and φ intends thus to find an ideal balance between the dynamic behavior and the machining time reduction.

Regarding the results in terms of remaining volume homogeneity, *Figure 13* details the distribution of remaining material along the CAD surfaces. The strategies which use an optimization of the tool axis orientation angle limits (case 3 and 4) lead to a lower scallop height thanks to the limiting of the effective cutting radius induced. Nevertheless, these values are very high and are all identified to be in the traveling of the corner 2 which is the more constraining considering the undercut areas involved. The high radial engagement of the tool worsen the scallop heights, which could then be reduced by reducing the radial engagement. The remaining material percentage values are sensibly equal for each strategy, which is normal given the fact that the tool travels along the same guide curves for all the tested strategies.

Finally, the strategy to apply depends on the machining application required, as a compromise cannot be found considering each optimization criterion. For example, when roughing in aluminium alloys, the productivity can be highlighted by a smoothness optimization. But in harder materials, such as titanium or nickel alloys, the guarantee of the tool lifespan prevails. In this case, the tool axis orientation limits optimization is preferable compared to the reducing of the machining time not to break the tool prematurely.

It can be noted that one of the strength of this optimization method lies in the possibility of optimizing each path with different optimization weights and then optimize productivity or remaining material homogeneity in function of the localization of the path in relation to the finished surfaces. By this way, the productivity would be promoted along the paths which does not machine a finish surface, and the homogeneity of remaining material would prevail along the paths which machine a finished surface.

5. Conclusion

Controlling the orientation of the tool axis is critical in a pocket roughing operation in 5-axis milling, where tool workpiece engagement is important. A strategy is therefore proposed to constrain the tool axis orientation along the entire trajectory. First, guide curves are used to constrain the tool orientation in the plane orthogonal to the feed direction, with maximum respect of the geometry of the flank surfaces. Then, a Sequential Quadratic Programming algorithm is used to carry out a three-objective optimization to constrain the orientation of the tool with respect to the end milled surface. It is thus possible to reduce machining times as well as the vibrations during roughing and depending on the weights assigned to each of the optimization objectives. In terms of perspectives, further studies could be carried out on the dynamic behavior of the tool, tool holder and spindle assembly and tool life according to the evolution of the tool axis orientation in rough machining.

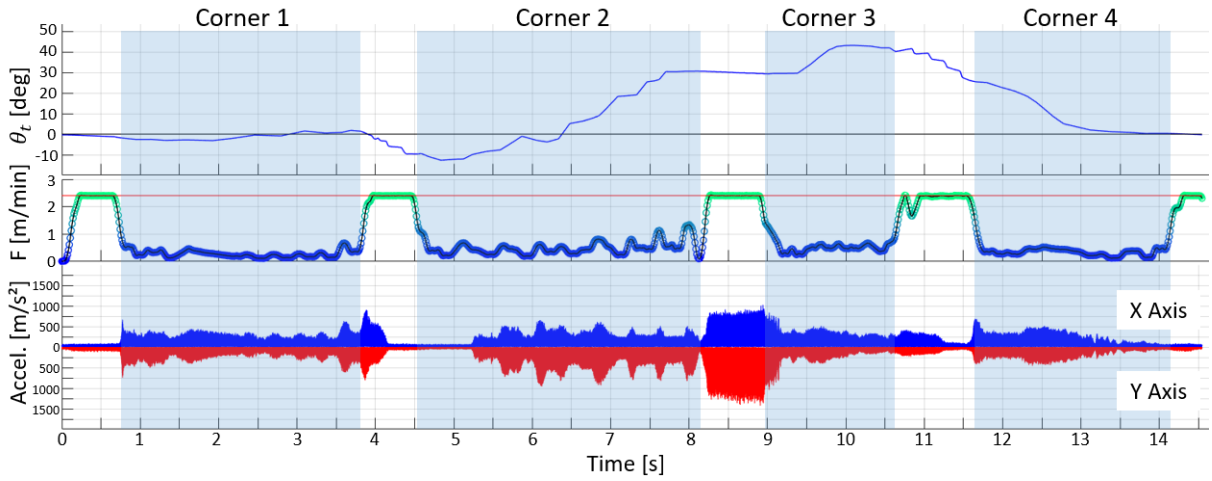

Figure 9: Case 1: uniform parametric synchronization ($\beta = 0, \varphi = 0, \tau = 0$)

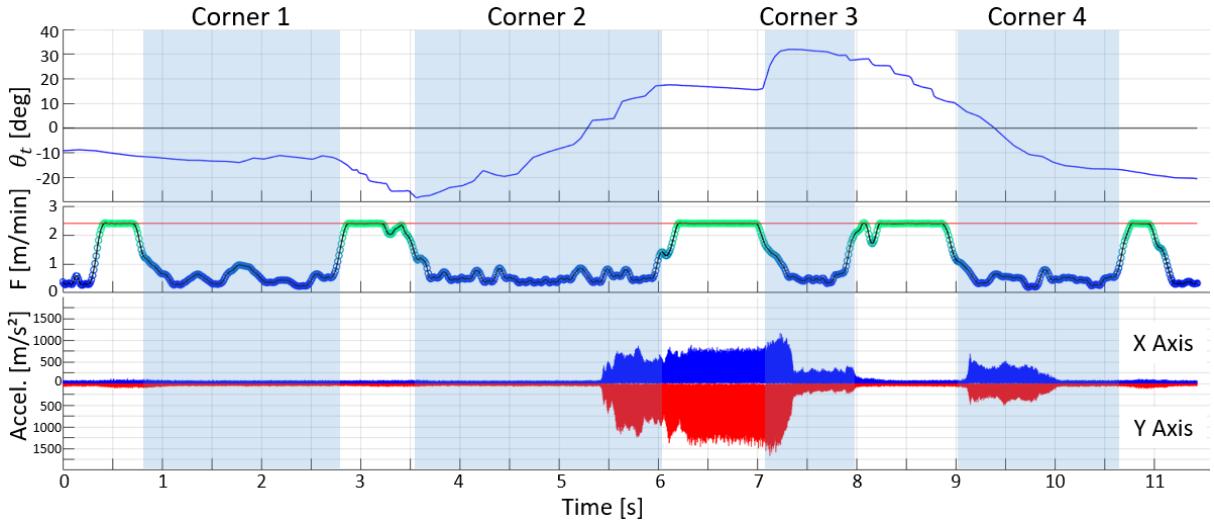

Figure 10: Case 2: smoothness optimization ($\beta = 0, \varphi = 1, \tau = 0$)

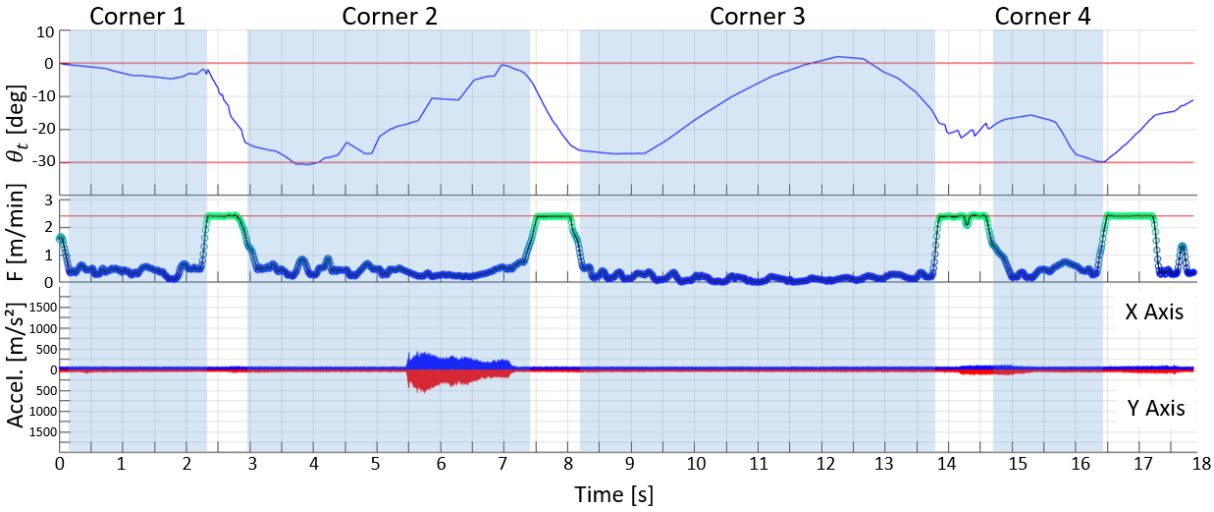

Figure 11: Case 3: limits optimisation ($\beta = 1, \varphi = 0, \tau = 0$)

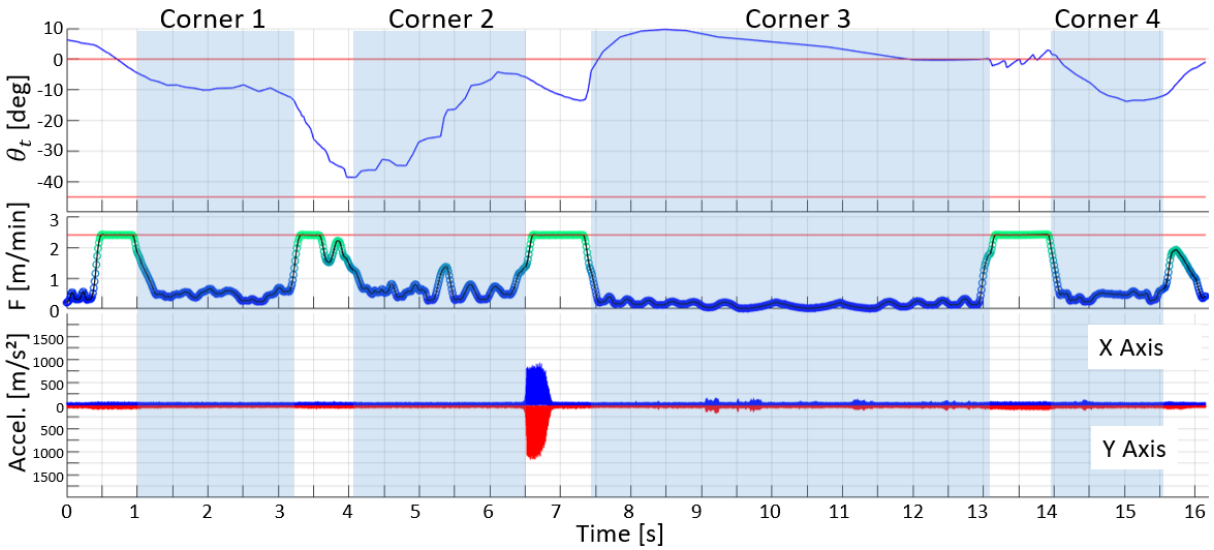

Figure 12: Case 4: combined optimisation ($\beta = 5, \varphi = 10, \tau = 0$)

[1] J. P. Davim. Machining of complex sculptured surfaces. Springer, 2012. https://doi.org/10.1007/978-1-4471-2356-9
[2] A. Krimpenis, G.-C. Vosniakos, The uniformity of remaining volume on rough-machined sculptured surface parts, The International Journal of Advanced Manufacturing Technology 43(2009) 896-906.
[3] D. Prat, G. Fromentin, G. Poulachon, and E. Duc. Experimental Analysis and Geometrical Modelling of Cutting Conditions Effect in 5 Axis Milling with Ti6Al4V Alloy. Procedia CIRP, 1(2012) 84-89.
[4] Y. Sun, Y. Bao, K. Kang, and D. Guo. A cutter orientation modification method for five-axis ball-end machining with kinematic constraints. The International Journal of Advanced Manufacturing Technology, 67(2013) 2863-2874.
[5] S. Lavernhe, C. Tournier, C. Lartigue, Optimization of 5-axis high-speed machining using a surface based approach, Computer-Aided Design 40 (10-11) (2008) 1015-1023.
[6] X. Pessoles, Y. Landon, S. Segonds, W. Rubio. Optimisation of workpiece setup for continuous five-axis milling: application to a five-axis BC type machining centre. The International Journal of Advanced Manufacturing Technology 65(1) (2013) 67-79.
[7] D. Plakhotnik and B. Lauwers. Graph-Based Optimization of Five-Axis Machine Tool Movements by Varying Tool Orientation. The International Journal of Advanced Manufacturing Technology, 74(1-4) (2014) 307-318.
[8] C. Castagnetti, E. Duc, and P. Ray. The domain of admissible orientation concept: A new method for five-axis tool path optimisation. Computer-Aided Design, 40(2008) 938-950.
[9] Lu, Y., Ding, Y., and Zhu, L. Smooth Tool Path Optimization for Flank Milling Based on the Gradient-Based Differential Evolution Method. ASME Journal of Manufacturing Science and Engineering 138 (8) (2016) 081009.
[10] X. Beudaert, P.-Y. Pechard, C. Tournier, 5-Axis tool path smoothing based on drive constraints, International Journal of Machine Tools and Manufacture, 51(2011) 958-965.
[11] X. Beudaert, S. Lavernhe, and C. Tournier. 5-axis local corner rounding of linear tool path discontinuities. International Journal of Machine Tools and Manufacture, 73(2013) 9-16.
[12] M.-C. Ho, Y.-R. Hwang, C.-H. Hu. Five-axis tool orientation smoothing using quaternion interpolation algorithm, International Journal of Machine Tools and Manufacture 43 (12) (2003) 1259-1267.
[13] P. -Y. Pechard, C. Tournier, C. Lartigue, and J.-P. Lugarini. Geometrical deviations versus smoothness in 5-axis high-speed flank milling. International Journal of Machine Tools and Manufacture, 49(2009) 454-461.
[14] L. Chen, K. Xu, and K. Tang. Collision-free tool orientation optimisation in five-axis machining of bladed disk. Journal of Computational Design and Engineering, 2(2015) 197-205.
[15] L.N. López de Lacalle, A. Lamikiz, J.A. Sánchez, and M.A. Salgado. Toolpath selection based on the minimum deflection cutting forces in the programming of complex surfaces milling. International Journal of Machine Tools and Manufacture, 47(2007) 388-400.
[16] C. -S. Jun, K. Cha, and Y. -S. Lee. Optimizing tool orientations for 5-axis machining by configuration-space search method. Computer-Aided Design, 35(2003) 549-566.
[17] P. Gilles, F. Monies, and W. Rubio. Optimum orientation of a torus milling cutter: Method to balance the transversal cutting force. International Journal of Machine Tools and Manufacture, 47(2007) 2263-2272.
[18] G. Kiswanto, H. Hendriko, and E. Duc. An analytical method for obtaining cutter workpiece engagement during a semi-finish in five-axis milling. Computer-Aided Design, 55(2014) 81-93.
[19] B. Jousselin, Y. Quinsat, and C. Tournier. A 5-axis pocket roughing strategy reducing the remaining material volume. Procedia CIRP, 82(2019) 368-373.
[20] P. E. Gill, W. Murray, and M. A. Saunders. SNOPT: An SQP Algorithm for Large-Scale Constrained optimisation. SIAM Review, 47(2005) 99-131.

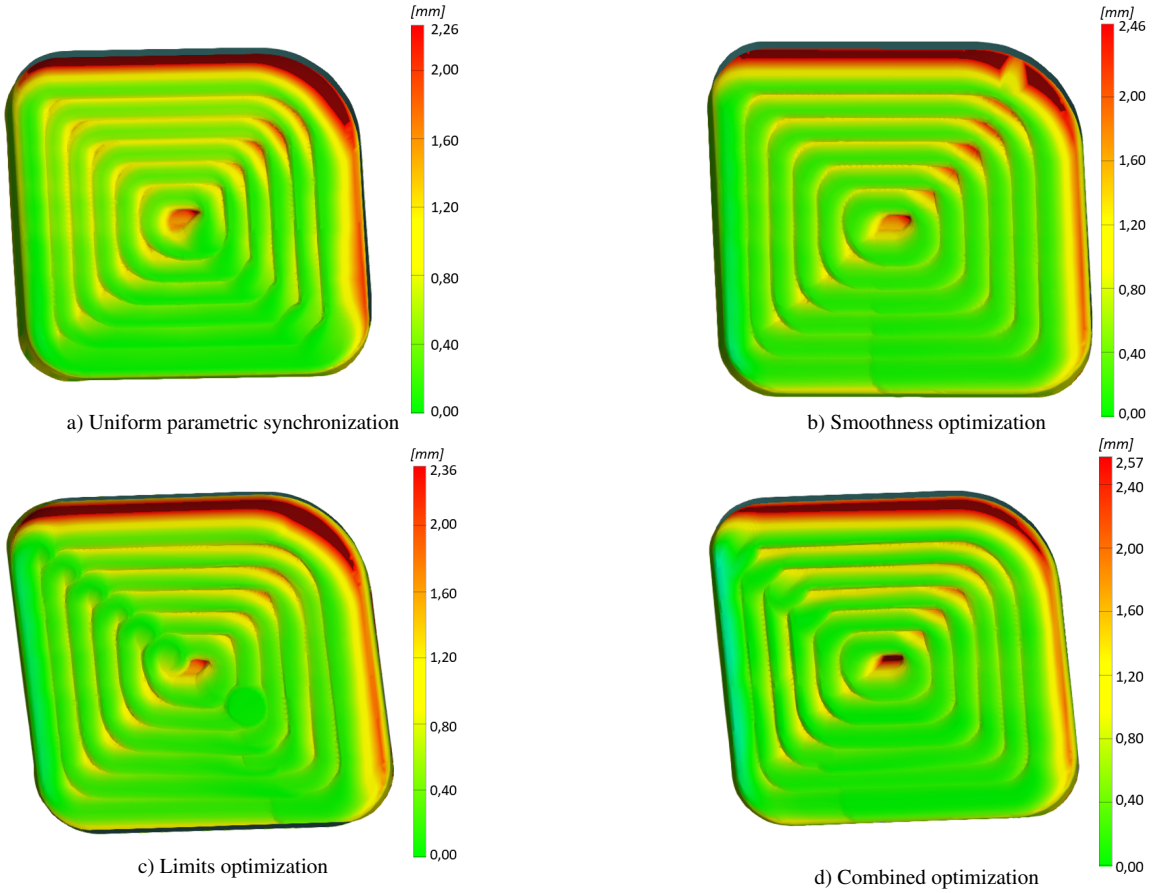

a) Uniform parametric synchronization

b) Smoothness optimization

c) Limits optimization

d) Combined optimization

Figure 13: Remaining material distribution after machining